**Electronic Supplementary Information**

# Ir single atoms and nanoclusters anchored on Ni aerogels for enhanced alkaline water oxidation: Unravelling the Ir coordination environment and the Ir-Ni synergistic effect

Jiacheng Chen, [a, b] Zihao Xie, [a, b] Chengyu Guo, [a] Xianxing Zhou,[a] Xiufang Wang [*, b] and Zhenghua Tang [*, a]

[a.] New Energy Research Institute, School of Environment and Energy, South China University of Technology, Guangzhou Higher Education Mega Centre, Guangzhou, 510006, China, zhht@scut.edu.cn

[b.] School of Pharmacy, Guangdong Pharmaceutical University, Guangzhou, 510006, China, x_f_wang@163.com

# Experimental section

## Reagents and materials

Ethanol (99.9%), ethylenediaminetetraacetic acid disodium salt dihydrate ($Na_2EDTA{\cdot}2H_2O$), iridium chloride trihydrate ($IrCl_3{\cdot}3H_2O$), and nickel chloride hexahydrate ($NiCl_2{\cdot}6H_2O$) were purchased from Energy Chemical Company, China. Sodium borohydride ($NaBH_4$) was purchased from Guangzhou Chemical Reagent Factory. All solutions were prepared by using deionized water. All the chemicals were used as purchased without further purification.

## Synthesis of Ni Aerogel

The synthesis of Ni aerogels was adapted from previous work.[1] Typically, 2 mmol of $NiCl_2{\cdot}6H_2O$ is dissolved in 120 mL of deionized water and 200 mmol of $NaBH_4$ is dissolved in 10 mL of deionized water. Subsequently, the $NaBH_4$ solution is rapidly injected into the $NiCl_2$ solution under sonication, and the sonication is maintained continuously for ~3-5 mins. The mixture was then left to age overnight, washed 3-5 times with ethanol and deionized water. The Ni Aerogel was obtained by freezing-dying overnight.

## Synthesis of Ir-EDTA@Ni Aerogel

The capture of iridium ions was adapted from previous studies.[2-6] Typically, 50 mg of Ni aerogel was dispersed in 10 mL of deionized water, 0.02836 mmol of EDTA, 50 μL of $IrCl_3$ solution (0.2836 mM) was added and sonicated to form a homogeneous solution. The solution was heated to 150 °C and held for 12 h. The black powder obtained was then washed several times with ethanol and water and dried to obtain the Ir-EDTA@Ni Aerogel.

## Synthesis of N/O@Ni Aerogel

Typically, 50 mg of Ni aerogel was dispersed in 10 mL of deionized water, 0.028 mmol of EDTA was also added. The mixture was sonicated to form a homogeneous solution. As a control sample, Ir element

is not added. The solution was heated to 150 °C and held for 12 h. The black powder was obtained, and then annealed under $Ar/H_2$ atmosphere, heated to 300°C and held for 2 h to form N/O@Ni Aerogel.

## Synthesis of Ir-SAs@Ni Aerogel

The Ir-EDTA@Ni aerogel prepared as above was annealed under $Ar/H_2$ atmosphere, heated to 300°C and held for 2 h to form Ir-SAs@Ni Aerogel.

## Characterization

The crystal structure of the samples was determined by powder X-ray diffraction (PXRD), collected on Empyrean by Cu $K_\alpha$ radiation source. Morphological and surface structural information of the samples was obtained by field emission scanning electron microscopy (FE-SEM, Merlin), transmission electron microscopy (TEM, Talos F200X), high-resolution TEM (HR-TEM), and high-angle annular dark field scanning TEM (HAADF-STEM) scans. Energy dispersive spectroscopy (EDS) elemental mapping was also used to measure the elemental distribution of the samples. The chemical composition and electronic structure of the samples were analyzed by X-ray photoelectron spectroscopy (XPS) results. The Quantachrome Autosorb-IQ2 Physical/Chemical Adsorbent Analyzer was employed for the purpose of testing and analysing the pore size distribution, specific surface area and pore structure of samples.

Ir L3-edge XAFS analysis were performed with Si(111) crystal monochromators at the BL14W Beam line at the Shanghai Synchrotron Radiation Facility (SSRF) (Shanghai, China). Before the analysis at the beamline, samples were placed into aluminum sample holders and sealed using Kapton tape film. The XAFS spectra were recorded at room temperature using a 4-channel Silicon Drift Detector (SDD) Bruker 5040. Ir L3-edge extended X-ray absorption fine structure (EXAFS) spectra were recorded in transmission mode. Negligible changes in the line-shape and peak position of Ir L3-edge XANES spectra were observed between two scans taken for a specific sample. The XAFS spectra of these standard samples were recorded in transmission mode. The spectra were processed and analyzed by the software codes Athena.

The XAFS data were processed according to the standard procedures using the Athena module implemented in the IFEFFIT software packages. The EXAFS spectra were obtained by subtracting the post-edge background from the overall absorption and then normalizing with respect to the edge-jump

step. Data reduction, data analysis, and EXAFS fitting were performed and analyzed with the Athena and Artemis programs of the Demeter data analysis packages (reference 1) that utilizes the FEFF6 program to fit the EXAFS data. The energy calibration of the sample was conducted through a standard Fe foil, which as a reference was simultaneously measured. A linear function was subtracted from the pre-edge region, then the edge jump was normalized using Athena software. The χ(k) data were isolated by subtracting a smooth, third-order polynomial approximating the absorption background of an isolated atom. The *k2*-weighted *χ(k)* data were Fourier transformed after applying a Hanning window function ($\Delta k$ = 1.0). For EXAFS modeling, the global amplitude EXAFS (*CN, R,* $\sigma^2$ and $\Delta E_0$) were obtained by nonlinear fitting, with least-squares refinement, of the EXAFS equation to the Fourier-transformed data in *R*-space, using Artemis software, EXAFS of the Ir foil is fitted and the obtained amplitude reduction factor $S_0^2$ value (0.760) was set in the EXAFS analysis to determine the coordination numbers (*CNs*) in scattering path in sample.

## Electrochemical measurements

All electrochemical tests were conducted on an electrochemical workstation (CHI 750E, Chenhua Instruments, China) utilizing a conventional three-electrode system consisting of an Hg/HgO electrode as the reference electrode and carbon rods as the counter electrode in a 1.0 M KOH aqueous solution at ambient temperature. 5.0 mg of the sample was dispersed in a 1.0 mL solution consisting of 30 μL of 5 wt% Nafion solution, 70 μL of deionized water, and 900 μL of ethanol and sonicated in an ice bath for 2 h to form a homogeneous catalyst ink, and then 18 μL of the catalyst ink was cast onto a glassy carbon electrode (0.125 $cm^2$) to prepare a working electrode. A carbon rod was employed as the counter and reference electrode and a Hg/HgO electrode was employed as reference electrode. The electrocatalytic activity was evaluated by linear sweep voltammetry (LSV) which was carried out at a scan rate of 5 mV $s^{-1}$ under 500 rpm stirring. The Tafel slope was calculated based on the following equation: $\eta = b \log j + a$, where η is overpotential, b is Tafel slope, a is the Tafel intercept, and j is current density. Electrochemical impedance spectroscopic (EIS) tests were performed from $10^5$ to $10^{-1}$ Hz with an alternating current amplitude of 5 mV. The CV curves were obtained by the CV method at different scan rates (5, 20, 40, 60, 80 and 100 mV $s^{-1}$) in the potential range of 1.025 to 1.125 V (vs. Hg/HgO), and then a straight line was obtained by linear fitting with the difference in current densities at the midpoint potential and the scan rate, and the slope of the straight line was $C_{dl}$. Further calculations of ECSA can be obtained through the equation: $ECSA = {C_{dl}}/{C_s}$, where ECSA represents the electrochemical active surface area of the catalyst and $C_s$ = 0.060 mF·$cm^{-2}$. Long-term durability of the samples was evaluated by *i*-t test. The specific activity and mass activity of the catalyst are calculated using the following equations to evaluate its intrinsic activity: $specific\ activity = {I}/{ECSA}$, where $I$ represents the current density at an overpotential of 300 mV. All curves were iR compensated (90%) to eliminate the effect of solution resistance.

## Computational details

All the computations were implemented with spin-polarized density functional theory (DFT) method, as performed by the Vienna ab initio simulation package (VASP).[7] The projector augmented wavefunction (PAW) pseudo-potentials are used to describe ionic potentials.[8] The exchange correlation energy is sculptured by Perdew–Burke–Ernzerhof (PBE) functional within the generalized gradient approximation (GGA).[9] In the course of the geometry relaxation, the energy cut-off was chosen as 500 eV, the Brillouin zone are sampled by 3 × 3 × 1 mesh points in k-space based on Monkhorst-Pack scheme both for Ni(111) and IrO-Ni(111) structures. The convergence criterion for the iteration in self-consistent field (SCF) is set to be 10−5 eV, and the force convergence criterion for atomic relaxation is set to be 0.02 eV /Å. Grimme's DFT-D3 methodology was used to describe the dispersion interactions. The vacuum gap is set as 15 Å to preclude interplay between two adjacent surfaces.[10]

The adsorption energy of intermediates (O*, OH* and OOH*) adsorbed on the Ru and RuIr is obtained by:

$$\Delta E_{ads} = E_{O*/OH*/OOH*} - E_{*} - E_{O/OH/OOH} \quad (1)$$

where $E_{*}$, $E_{O^{*}}$, $E_{OH^{*}}$ and $E_{OOH^{*}}$ stand for the total energies of the catalyst substrate without and with the adsorption of O, OH and OOH, respectively. The energies of O, OH and OOH are calculated from the energies of $H_2O$ and $H_2$ molecules in gas phases. By adopting the computational hydrogen electrode (CHE) model developed by Nørskov et al., the Gibbs free energy (ΔG) of each adsorbate is calculated by the expression:[11]

$$\Delta G = \Delta E_{ads} + \Delta ZPE - T\Delta S \quad (2)$$

where $\Delta E_{ads}$ is the adsorption energy obtained from DFT calculation, ΔZPE is the zero-point energy correction, T is the temperature (298.15K), ΔS is the entropy change. The entropies and vibrational frequencies of the species in gas phase are taken from NIST database.

The oxygen evolution reaction (OER) elementary steps take the reverse direction of ORR, and also consist of four element steps:

(i) $OH^{-} = HO^{*} + e^{-}$

(ii) $HO^{*} + OH^{-} = O^{*} + H_2O\,(l) + e^{-}$

(iii) $O^{*} + OH^{-} = OOH^{*} + e^{-}$

(iv) $OOH^{*} + OH^{-} = O_2\,(g) + H_2O\,(l) + e^{-}$

where (l) and (g) refer to liquid and gas phases, respectively.

The theoretical overpotentials for O OER ($\eta^{OER}$) can be computed by the equation as follows:

$$\eta^{OER} = max(\triangle Gi, \triangle Gii, \triangle Giii, \triangle Giv)/e - 1.23 \quad (2)$$

## Supplementary Figures

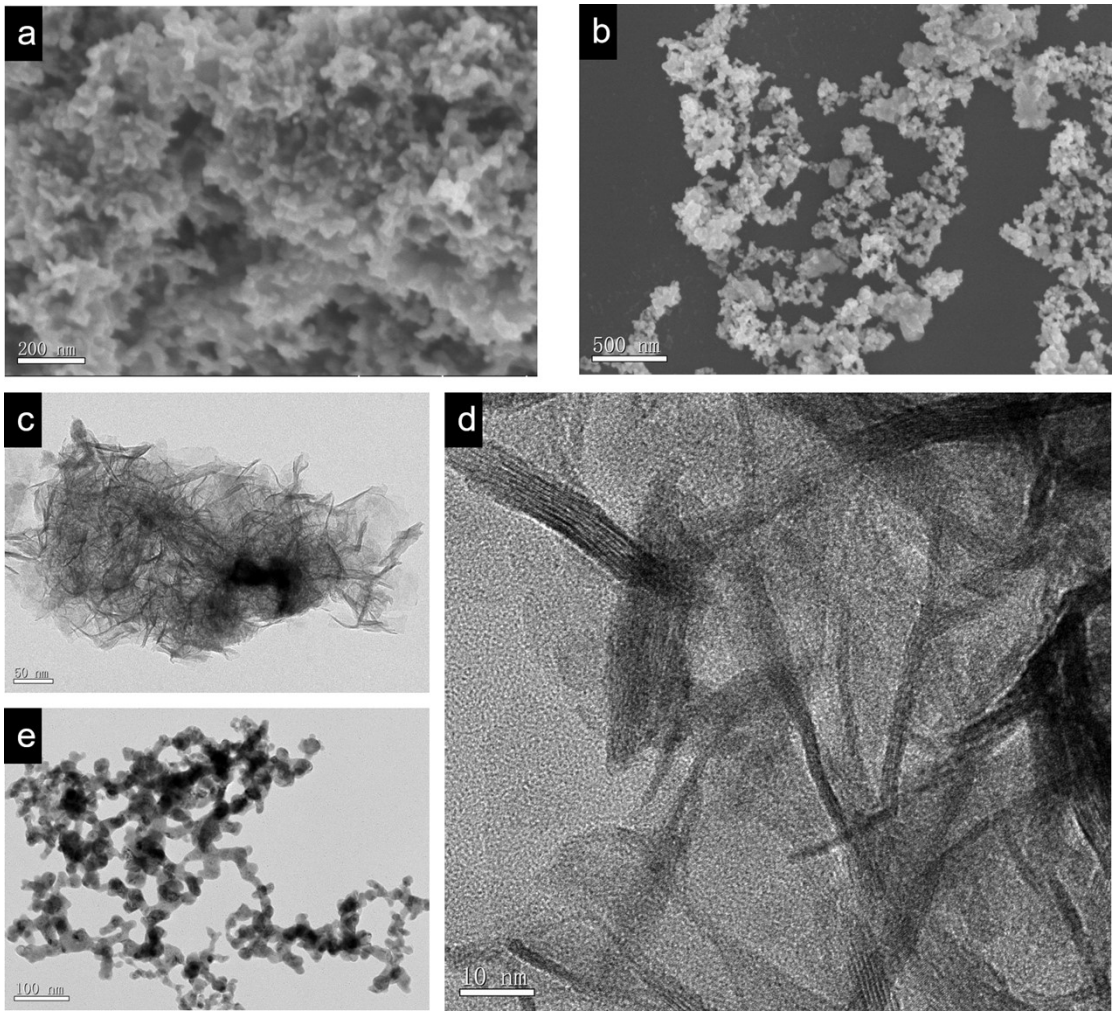


**Fig. S1** Typical SEM image of (a) Ir-EDTA@Ni Aerogel and (b) Ni Aerogel; Typical TEM image of (c-d) Ir-EDTA@Ni Aerogel with different magnifications and (e) Ni Aerogel.

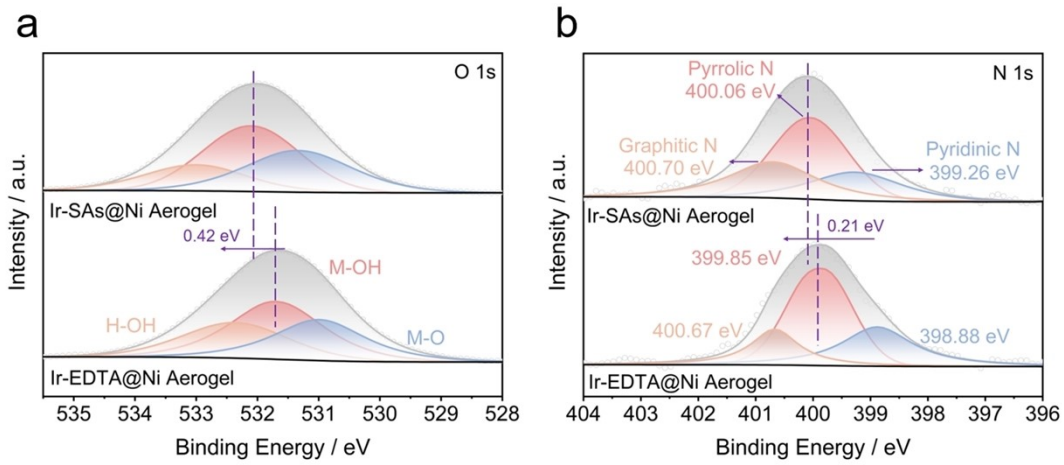


**Fig. S2** The high-resolution (a) O 1s and (b) N 1s XPS spectra of Ir-SAs@Ni Aerogel and other comparative samples.

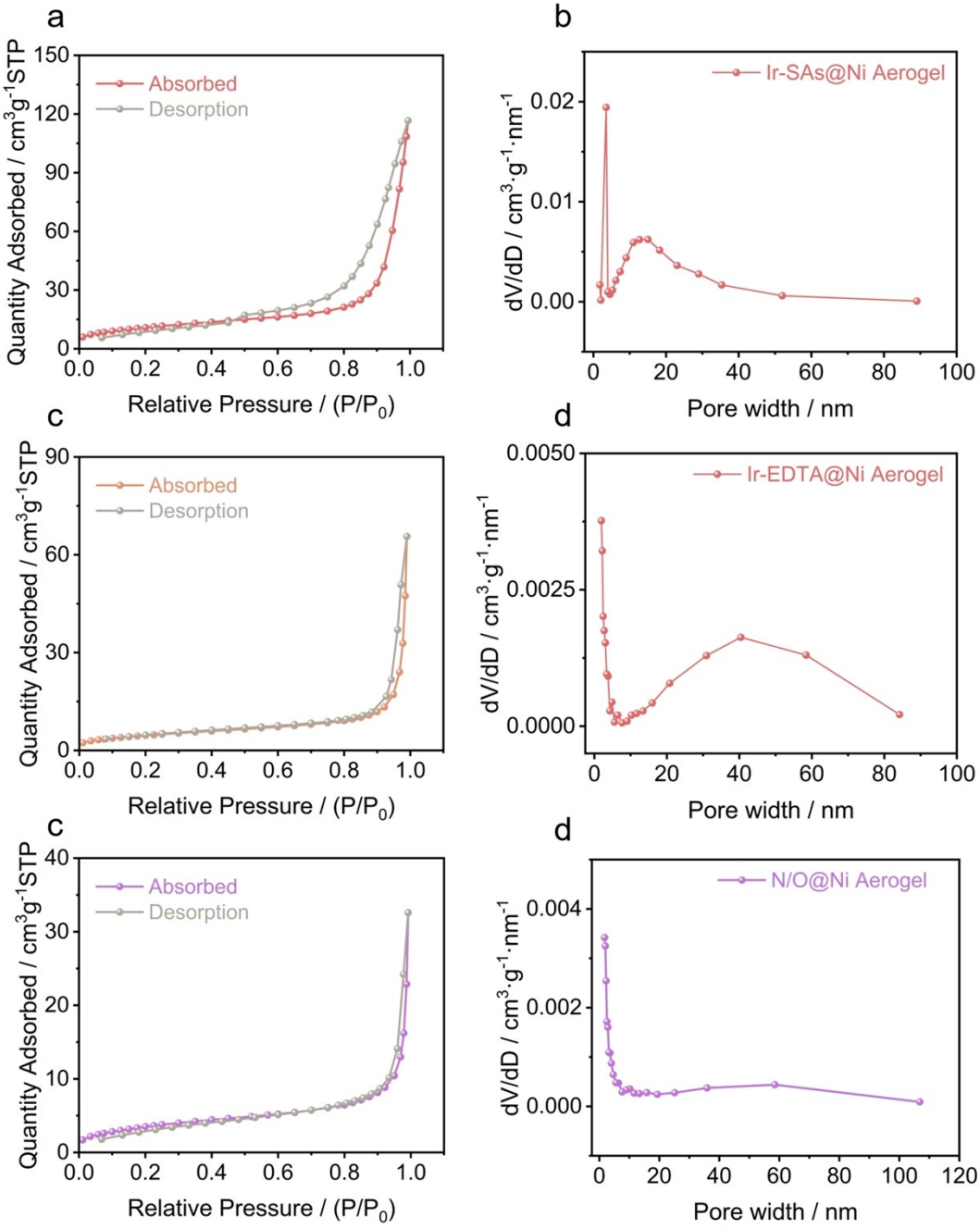


**Fig. S3** $N_2$ adsorption/desorption isotherms and corresponding pore-size distribution of (a-b) Ir-SAs@Ni Aerogel, (c-d) Ir-EDTA@Ni Aerogel and (e-f) N/O@Ni Aerogel.

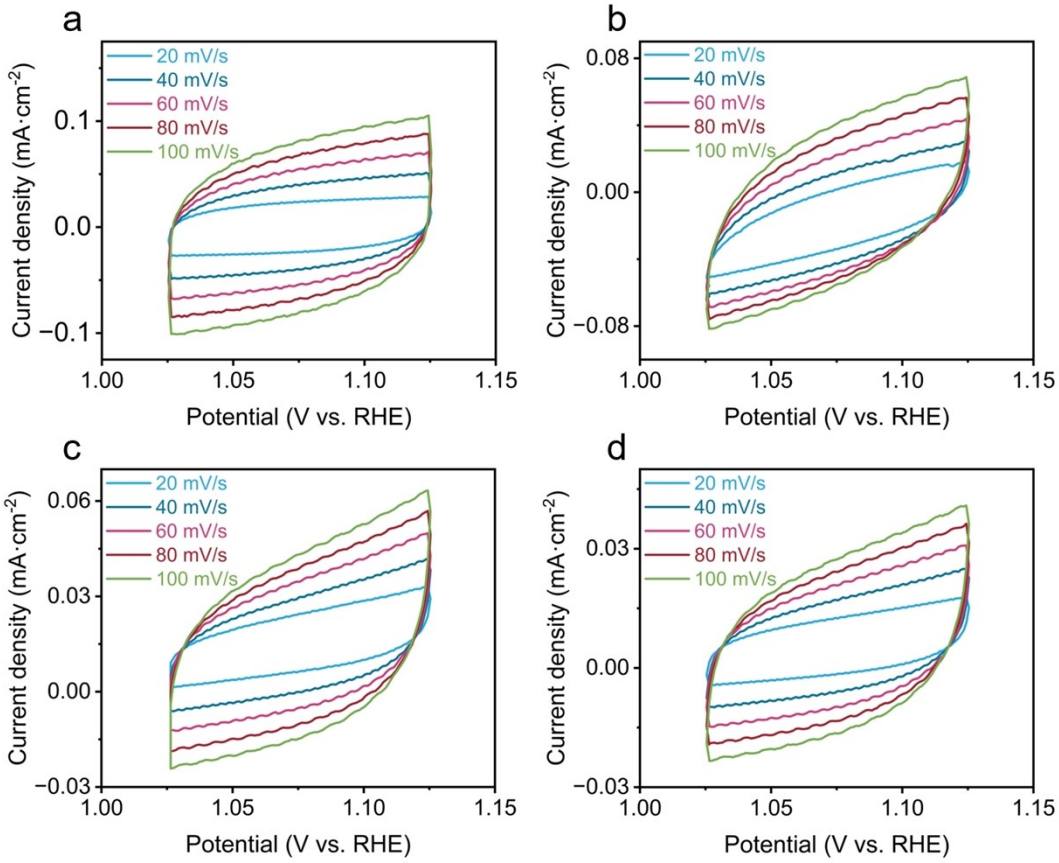


**Fig. S4** Cyclic voltammograms of the (a) Ir-SAs@Ni Aerogel, (b) Ir-EDTA@Ni Aerogel, (c) N/O@Ni Aerogel and (d) Ni Aerogel in the potential range from 1.025 to 1.125 V (vs. Hg/ HgO) at different scan rates.

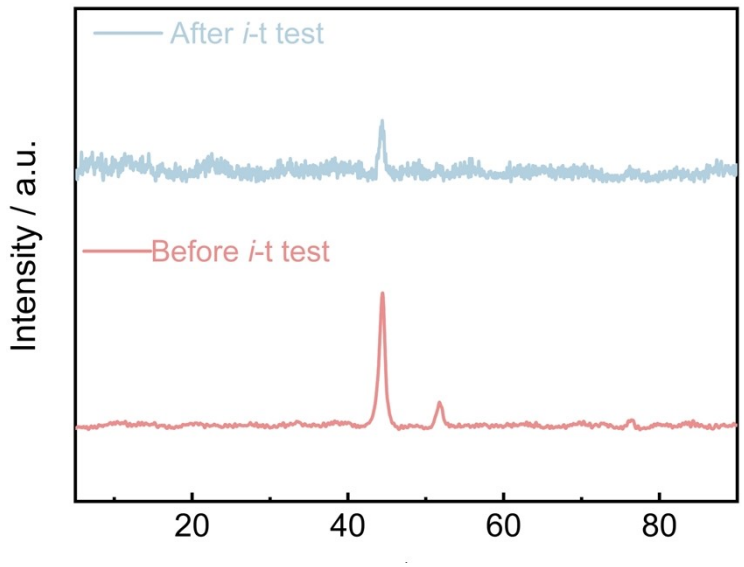


**Fig. S5** XRD pattern of Ir-SAs@Ni Aerogel before and after the *i*-t test.

## Supplementary Tables

**Table S1** The relevant parameters of BET test.

| Sample | BET Surface Area | BJH Desorption average pore diameter |
|---|---|---|
| Ir-SAs@Ni Aerogel | 39.72 m²/g | 15.20 nm |
| Ir-EDTA@Ni Aerogel | 17.20 m²/g | 24.78 nm |
| N/O@Ni Aerogel | 13.11 m²/g | 15.71 nm |

**Table S2** The EXAFS fitting parameters at the Ir *L3*-edge for various samples ($S_0^2$ = 0.76).

| Sample | Shell | *CN*[a] | *R*(Å)[b] | $\sigma^2$(Å$^2$)[c] | $\Delta E_0$ (eV)[d] | *R* factor |
|---|---|---|---|---|---|---|
| Ir foil | Ir-Ir | 12* | 2.71 ± 0.01 | 0.0029 | 8.2 ± 0.5 | 0.0027 |
| Ir-SAs@Ni Aerogel | Ir-O | 4.5 ± 0.1 | 2.01 ± 0.01 | 0.0062 | 13.6 ± 0.7 | 0.0041 |
| | Ir-Ni | 1.3 ± 0.3 | 2.45 ± 0.02 | 0.0156 | | |
| | Ir-O-Ir | 4.2 ± 1.2 | 3.12 ± 0.03 | 0.0176 | | |
| $IrO_2$ | Ir-O | 6.0 ± 0.2 | 1.98 ± 0.01 | 0.0018 | 13.8 ± 0.9 | 0.0086 |
| | Ir-Ir | 3.1 ± 0.6 | 3.15 ± 0.02 | 0.0030 | | |
| | Ir-Ir1 | 8.4 ± 1.4 | 3.54 ± 0.01 | 0.0041 | | |
| | Ir-O1 | 6.0 ± 1.7 | 3.58 ± 0.03 | 0.0011 | | |

[a]*CN*, coordination number; [b]*R*, the distance to the neighboring atom; [c]$\sigma^2$, the Mean Square Relative Displacement (MSRD); [d]$\Delta E_0$, inner potential correction; *R* factor indicates the goodness of the fit. $S0^2$ was fixed to 0.76, according to the experimental EXAFS fit of Ir foil by fixing *CN* as the known crystallographic value. * This value was fixed during EXAFS fitting, based on the known structure of Ir. Fitting range: 3.0 ≤ *k* (/Å) ≤ 14.2 and 1.0 ≤ *R* (Å) ≤ 3.0 (Ir foil); 3.0 ≤ *k* (/Å) ≤ 10.4 and 1.2 ≤ *R* (Å) ≤ 3.5 (sample); 3.0 ≤ *k* (/Å) ≤ 10.3 and 1.2 ≤ *R* (Å) ≤ 3.5 (sample2); 3.0 ≤ *k* (/Å) ≤ 11.9 and 1.0 ≤ *R* (Å) ≤ 4.0 ($IrO_2$). A reasonable range of EXAFS fitting parameters: 0.700 < $S_0^2$ < 1.000; *CN* > 0; $\sigma^2$ > 0 Å$^2$; $|\Delta E_0|$ < 20 eV; *R* factor < 0.02.

**Table S3** The OER activity comparison between Ir-SAs@Ni Aerogel and recently reported top-level OER catalysts in 1.0 M KOH.

| Catalyst | $\eta_{10}$ (mV) | Tafel slope (mV·dec$^{-1}$) | Reference |
|---|---|---|---|
| Ir-SAs@Ni Aerogel | 281 | 64.36 | This work |
| Ir-EDTA@Ni Aerogel | 340 | 93.79 | This work |
| Ni Aerogel | 364 | 120.45 | This work |
| $IrO_2$ | 322 | 89.79 | This work |
| Fe-SAC@COF | 290 | 40 | [1] |
| Ni–O–G SACs | 328 | 84 | [12] |
| Ni@NiNCNT | 358 | 89 | [13] |
| Ni-SAs@NC | 356 | - | [14] |
| Ni SAs-Pd@NC (2:1) | 360 | 79 | [15] |
| Ir-rEGO | 294 | - | [16] |
| CoMM | 351 | 84 | [17] |
| P-CoPc@CNT | 300 | 41.7 | [18] |
| $Co_{SA}$/CNF | 390 | 74 | [19] |
| CoO/$Ru_{1.25\%}$HPN | 308 | 308 | [20] |

**Table S4** Fitting parameters obtained from the EIS data for the OER in 1.0 M KOH.

| Catalysts | $R_S$ (Ω) | CPE1-T | CPE1-P | R1 (Ω) | CPE2-T | CPE2-P | R2 (Ω) |
|---|---|---|---|---|---|---|---|
| Ir-SAs@Ni Aerogel | 7.265 | 0.000138 | 0.758 | 2.619 | 0.0173 | 0.819 | 5.151 |
| Ir-EDTA@Ni Aerogel | 7.817 | 0.00358 | 0.542 | 5.204 | 0.00262 | 0.838 | 22.350 |
| N/O@Ni Aerogel | 7.559 | 0.0002465 | 0.739 | 2.437 | 0.0028649 | 0.88683 | 31.01 |
| Ni Aerogel | 7.468 | 0.000559 | 0.653 | 2.915 | 0.00252 | 0.930 | 49.520 |
| $IrO_2$ | 7.553 | 0.0164 | 0.376 | 3.038 | 0.00226 | 0.892 | 16.530 |

$R_S$: Solution resistance;

R1: Charge-transfer resistance;

R2: Solid-electrolyte interface resistance;

CEP1: Capacitance generated from the Faradic process, and constant-phase element;

CEP2: Capacitance arisen from the solid-electrolyte interface process.[21]

**Table S5** The calculated specific activity and mass activity at an overpotential of 300 mV for all the samples.

| Sample | $C_{dl}$ / mF·cm$^{-2}$ | $C_S$ / mF·cm$^{-2}$ | ECSA | $\eta$ / mV | I / mA·cm$^{-2}$ | m / mg | Specific Activity / mA·cm$^{-2}$ | Mass Activity / mA·mg$^{-1}$ |
|---|---|---|---|---|---|---|---|---|
| Ir-SAs@Ni Aerogel | 1.420 | | 23.667 | | 20.392 | | 0.861 | 226.578 |
| Ir-EDTA@Ni Aerogel | 0.751 | 0.060 | 12.517 | 300 | 2.595 | 0.09 | 0.207 | 28.833 |
| N/O@Ni Aerogel | 0.493 | | 8.217 | | 1.239 | | 0.151 | 13.767 |

## References


1. J. Chen, Z. Xie, Y. Tang, Z. Tang and X. Wang, *New J. Chem.*, 2024, **48**, 13950-13956.
2. A. Savini, A. Bucci, M. Nocchetti, R. Vivani, H. Idriss and A. Macchioni, *ACS Catal.*, 2014, **5**, 264-271.
3. J. Jeskey, Y. Ding, Y. Chen, Z. D. Hood, H. Li, G. E. Sterbinsky and Y. Xia, *ChemCatChem*, 2024, **16**, e202400499.
4. A. Savini, G. Bellachioma, S. Bolano, L. Rocchigiani, C. Zuccaccia, D. Zuccaccia and A. Macchioni, *ChemSusChem*, 2012, **5**, 1415-1419.
5. J. Wang, Z. Wu, L. Han, C. Xuan, J. Zhu, W. Xiao, J. Wu, H. L. Xin and D. Wang, *Sustain. Energy Fuels*, 2017, **1**, 823-831.
6. L. Huang, N. Wang, M. Qi, Z. Liu, Z. Xu, Q. Zhang, Z. Shu, S. Shan, Y. Bian, J. Chen and Y. Jiao, *Int. J. Hydrogen Energy*, 2024, **88**, 1217-1225.
7. G. Kresse and J. Furthmüller, *Physical Review B*, 1996, **54**, 11169-11186.
8. G. Kresse and D. Joubert, *Phys. Rev. B*, 1999, **59**, 1758-1775.
9. J. P. Perdew, K. Burke and M. Ernzerhof, *Phys. Rev. Lett.*, 1996, **77**, 3865-3868.
10. S. Kattel, P. Atanassov and B. Kiefer, *J. Phys. Chem. C*, 2012, **116**, 8161-8166.
11. J. K. Nørskov, J. Rossmeisl, A. Logadottir, L. Lindqvist, J. R. Kitchin, T. Bligaard and H. Jónsson, *J. Phys. Chem. B*, 2004, **108**, 17886-17892.
12. Y. Xu, W. Zhang, Y. Li, P. Lu and Z.-S. Wu, *J. Energy Chem.*, 2020, **43**, 52-57.
13. X. Zhang, S. Feng, J. Yu, R. Shi, Z. Ma, Z. Yang and L. Yang, *Energy Fuels*, 2022, **36**, 13159-13167.
14. F. Luo, J. Zhu, S. Ma, M. Li, R. Xu, Q. Zhang, Z. Yang, K. Qu, W. Cai and Z. Chen, *Energy Storage Mater.*, 2021, **35**, 723-730.
15. S. Wang, Z. Lin, M. Li, Z. Yu, M. Zhang, M. Gong, Y. Tang and X. Qiu, *J. Mater. Chem. A*, 2022, **10**, 6086-6095.
16. X. Li, J. Cao, J. Chen, Y. Zhu, H. Xia, Z. Xu, C. Gu, J. Xie, M. Jones, C. Lyu, J. Corbin, X. Li and W. Hu, *Adv. Funct. Mater.*, 2024, **34**, 2313530.
17. P. Kumar, K. Kannimuthu, A. S. Zeraati, S. Roy, X. Wang, X. Wang, S. Samanta, K. A. Miller, M. Molina, D. Trivedi, J. Abed, M. A. Campos Mata, H. Al-Mahayni, J. Baltrusaitis, G. Shimizu, Y. A. Wu, A. Seifitokaldani, E. H. Sargent, P. M. Ajayan, J. Hu and M. G. Kibria, *J. Am. Chem. Soc.*, 2023, **145**, 8052-8063.
18. Y. Liu, S. Zhang, C. Jiao, H. Chen, G. Wang, W. Wu, Z. Zhuo and J. Mao, *Adv. Sci.*, 2023, **10**, 2206107.
19. J. Li, J. Zhu, Z. Jia, R. Li and J. Yu, *Chem- Asian J.*, 2023, **18**, e202300393.
20. W. Chen, Y. Song, L. Li, J. Guo and Z. Lin, *J. Energy Chem.*, 2024, **89**, 355-363.
21. W. Xue and W. Lin, *J. Colloid. Interface Sci.*, 2025, **700**, 138319.